arXiv:cond-mat/0210216v1 [cond-mat.stat-mech] 9 Oct 2002

Numerical study of a first-order irreversible phase transition in a $CO + NO$ catalyzed reaction model.

Ernesto S. Loscar[a] and Ezequiel V. Albano[a]
[a]*Instituto de Investigaciones Fisicoquímicas Teóricas y Aplicadas (INIFTA), UNLP, CONICET, Suc.4, CC16, 1900 La Plata, Argentina*

March 22, 2022

Abstract

The first-order irreversible phase transitions (IPT) of the Yaldran-Khan model (Yaldran-Khan, J. Catal. **131**, 369, 1991) for the $CO + NO$ reaction is studied using the constant coverage (CC) ensemble and performing epidemic simulations. The CC method allows the study of hysteretic effects close to coexistence as well as the location of both the upper spinodal point and the coexistence point. Epidemic studies show that at coexistence the number of active sites decreases according to a (short-time) power law followed by a (long-time) exponential decay. It is concluded that first-order IPT's share many characteristic of their reversible counterparts, such as the development of short ranged correlations, hysteretic effects, metastabilities, etc.

1 Introduction

The study of critical phenomena occurring in adsorbed overlayers is a topic that has attracted increasing attention [1]. In fact, the understanding of the behavior of atoms and molecules absorbed on different surfaces is essential for many branches of science (chemistry, physics, biology, etc). Within this wide context, surface phenomena occurring under non-equilibrium conditions are far from being understood. Therefore, they have become the center of great attention [2]. In particular, irreversible catalytic reactions exhibit a very rich and complex behavior that includes oscillations, bifurcations, chaos metastability, irreversible phase transitions (IPT's), etc. [3, 4, 5, 6, 7, 8, 9].

The aim of this work is to perform an extensive numerical study of the first-order IPT characteristic of a model for the $NO + CO$ reaction early proposed by Yaldran and Khan (YK) [4]. IPT's in reactive systems take place between an active regime with sustained

outcome of the reaction product from the catalytic surface and an absorbing (or poisoned) state where the catalyst becomes fully covered by one or more types of reactants. Since the systems cannot escape from the absorbing state the transitions are irreversible [2, 5, 6]. The study of IPT's has gained increasing attention in the field of nonequilibrium statistical physics since the pioneering work of Ziff, Gulari and Barshad (ZGB) that introduced a simple lattice model for the catalytic oxidation of CO [7]. Particularly interesting are first-order IPT's that can be characterized by an abrupt change in the density of reactants and in the rate of production due to a tiny change in the (external) control parameter, which is usually the pressure. In fact, evidence of such kind of transition has been reported in catalyzed reactions [8, 9]. The occurrence of hysteretic effects around a first-order transition point has also been observed [10]. Very recently, we have performed a detailed study of the first-order IPT of the ZGB model presenting conclusive evidence of hysteretic effects [11]. As anticipated above, the aim of this work is to characterize the first order IPT of the YK model [4] for the $CO+NO$ reactions by means of Monte Carlo simulations with particular emphasis on the occurrence of hysteretic effects and by performing useful comparisons with our previous study of the ZGB model [11].

The manuscript is organized as follows: in Section II we describe the YK model and three different simulation methods used in the work, namely the standard ensemble, the constant coverage ensemble and the epidemic approach. In Section III we present and discuss the obtained results, while our conclusions are stated in Section IV.

2 The model and Monte Carlo simulation methods.

2.1 The YK model for the $CO + NO$ reaction.

Yaldran and Khan [4] have proposed a lattice gas model for the catalytic reaction of $CO + NO$ based on the Langmuir-Hinshelwood mechanism. The reaction steps are as follows:

$$NO(g) + 2S \rightarrow N(a) + O(a) \tag{1}$$

$$CO(g) + S \rightarrow CO(a) \tag{2}$$

$$CO(a) + O(a) \rightarrow CO_2(g) + 2S \tag{3}$$

$$N(a) + N(a) \rightarrow N_2(g) + 2S \tag{4}$$

where S represents an unoccupied site on the catalyst surface, $2S$ represents a nearest neighbor (NN) pair of such sites, (g) indicates a molecule in the gas phase and (a) indicates an species adsorbed on the catalyst. The reactions given by equations (3) and (4) are assumed to be instantaneous (infinity reaction rate limit) while the limiting steps are the adsorption events given by equations (1) and (2). The YK model is similar to the ZGB model for the $CO + O_2$ reaction, except that the O_2 is replaced by NO, and NN

N atoms, as well as NN $CO - O$ pairs, react. For further details on the YK model see [4, 12, 13, 14, 15].

2.2 Monte Carlo simulation method using the standard ensemble

Monte Carlo simulations are performed on the hexagonal (triangular) lattice of side L, assuming periodic boundary conditions. In the standard ensemble the procedure is as follow: let P_{NO} and P_{CO} be the relative impingement rates for NO and CO, respectively, which are taken to be proportional to their partial pressures in the gas phase. Taking $P_{CO} + P_{NO} = 1$, such normalization implies that the YK model has a single parameter that is usually taken to be P_{CO}. CO and NO adsorption events are selected at random with probabilities P_{CO} and $1 - P_{CO}$, respectively. Subsequently, an empty site of the lattice is also selected at random. If the selected species is CO, the adsorption on the empty site occurs according to equation (2). If the selected molecule is NO, a NN site of the previously selected one is also chosen at random, and if such site is empty the adsorption event takes place according to equation (1). Of course, if the NN chosen site is occupied the adsorption trial is rejected. After each successful adsorption event all NN sites of the adsorbed species are checked at random for the occurrence of the reaction events described by equations (3) and (4).

The Monte Carlo time step (MCS) involves L^2 adsorption attempts, so that every site of the lattice is selected once, on average. Simulations are started with empty lattices. The first 10^4 MCS are disregarded to allow the system to reach the stationary regime and subsequently, averages are taken over 4 x 10^4 MCS. During the simulations, the coverages with CO, O and N (θ_{CO}, θ_O and θ_N, respectively) as well as the rate of production of CO_2 and N_2 (R_{CO_2}, R_{N_2}, respectively) are measured. The phase diagram of the YK model is similar to that of the ZGB model [7], in the sense that both second- and first- order IPT's are observed. However, in contrast to the ZGB model where the absorbing (poisoned) states are unique, in the case of the YK such states are mixtures of $O(a) + N(a)$ and $CO(a) + N(a)$ as follows from the observation of the left and right sides of the phase diagram, respectively (figure 1(a)).

The IPT observed close to $P^1_{CO} = 0.184(1)$ is continuous and therefore of second-order (see figure 1). Our estimation of P^1_{CO} is in agreement with previous calculations, namely $P^1_{CO} = 0.185(5)$ (reference [12]) and $P^1_{CO} = 0.185(2)$ (reference[4]).

More interesting, an abrupt first-order IPT is also observed close to $P^2_{CO} = 0.3545(5)$ (figure 1(a) and (b)), in agreement with previous simulations (references [4, 12]). It should be noticed that a reactive window for the YK model is observed on the hexagonal lattice (see figure 1) while such window is absent on the square lattice [4, 12], pointing out the relevance of the coordination number on the reactivity.

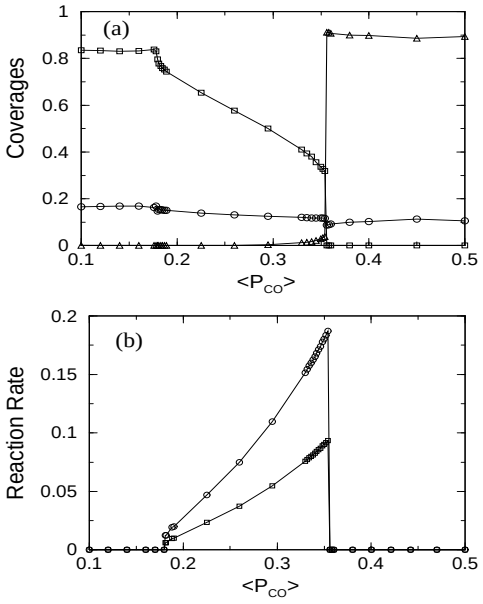


Figure 1: Phase diagram of the YK model on the hexagonal lattice of size L=128 LU. (a) Plots of $\theta_{CO}(\triangle)$, $\theta_O(\square)$ and $\theta_N(\bigcirc)$ versus $< P_{CO} >$. (b) Plots of $R_{N_2}(\square)$ and $R_{CO_2}(\bigcirc)$; measured in units of number of N_2 and CO_2 molecules removed from the lattice per unit of area and time, respectively; versus $< P_{CO} >$.

2.3 The constant coverage ensemble

The constant coverage ensemble (CC) was early introduced by Ziff and Brosilow [16] to study the first-order IPT of the ZGB model. The first step of the CC ensemble is to obtain a stationary configuration using the standard ensemble. Then the system is actually switched to the CC ensemble, where the density θ_{CO} is now kept as constant as possible. For this purpose, if θ_{CO} is below the established value, CO is adsorbed on a randomly selected site. Otherwise, if θ_{CO} is greater than the desired value, NO adsorption attempts on randomly selected sites are performed. Now the effective CO-pressure ($< P_{CO} >$) is given by the ratio of CO-adsorption attempts to the total number of adsorption attempts.

It is worth mentioning that using the CC method as proposed by Ziff and Brosilow [16], the actual coverage with CO is not strictly constant but it is affected by fluctuations of the order of $\approx 1/L^2$. Very recently [17], a true constant coverage ensemble, where the number of particles remains strictly constant, has been proposed and used to study the conserved contact process. This new method seems to be very useful for the study of single particle systems, such as the contact process, branching annihilating walkers, etc., although their implementation for complex multiparticle systems, such as the YK model, does not appear to be straightforward.

In simulations, $< P_{CO} >$ is averaged over τ_M time steps. Subsequently, θ_{CO} is increased stepwise and measurements of $< P_{CO} >$ are performed after some waiting time τ_W to allow the relaxation of the system. In this way the growing branch (GB) of the CC loop can be obtained. Then, after reaching a large value of θ_{CO} ($\theta_{CO} \approx 0.88$ in this work in order to prevent the system from reaching an absorbing state as shown in figure 1), θ_{CO} is decreased stepwise. Using this procedure the decreasing branch (DB) of the CC loop can be recorded. It should be noticed that in the CC ensemble θ_{CO} assumes the role of the control parameter. Further details on the CC method can be found in references [6, 11].

2.4 Epidemic simulations close to coexistence.

Another powerful approach to the study of IPT's is to perform the so-called epidemic analysis (EA) [18, 19]. In EA the simulations start from a configuration very close to the absorbing state and subsequently the time evolution of the system is followed using the standard ensemble (SE). In order to generate the initial configuration, a natural absorbing state has to be achieved first using the SE and following the dynamics of the system. This procedure assures the development of the characteristic correlations among the reactants. Taking the obtained absorbing state, a small patch of empty sites is created close to the center of the sample. Subsequently, during the time evolution of the system the average number of empty sites ($N(t)$) and the survival probability $P(t)$ of the active state are recorded. Each single EA stops when the system is trapped in the absorbing state so that $N(t) = 0$. In order to obtain reliable results, the quantities of interest have to be averaged over a large number of independent EA ($\sim$3x10^9 runs in the present work).

Performing EA close the second-order IPT the scaling ansatz $N(t) \propto t^{\eta}$, where η is an exponent, has been proposed to hold at criticality [18, 19]. This observation is in agreement with well established ideas developed by studying equilibrium (reversible) phase transition: scale invariance reflects the existence of a divergency in the correlation length. However, close to first-order transition it is also well known that correlations are short ranged, preventing the observation of scale invariance. Recently Monetti and Albano [11] have proposed that, at coexistence, $N(t)$ should decrease according to a short-time power law followed by a long-time exponential decay, so that:

$$N(t) \propto (\frac{t}{T})^{-\eta_{eff}} \exp[-(\frac{t}{T})] \tag{5}$$

where T sets a characteristic crossover time scale and η_{eff} is an effective exponent. It should be noticed that equation (5) holds for the ZGB model at coexistence [11].

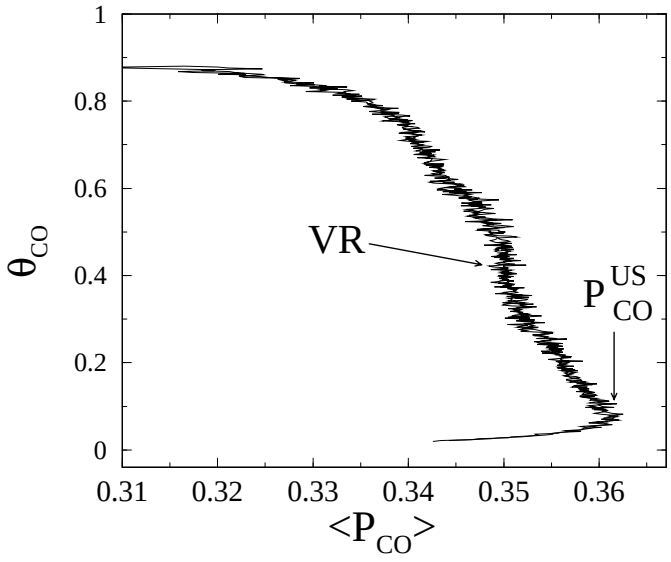


Figure 2: Plots of θ_{CO} versus $< P_{CO} >$ obtained using the CC ensemble with $L = 32$ LU, $\tau_R = 50$ MCS and $\tau_M = 50$ MCS. The arrows show the narrow vertical region of the loops (VR) and the upper spinodal point (P_{CO}^{US}), respectively. More details in the text.

3 Results and discussion.

3.1 Study of the hysteretic effects using the CC ensemble.

In order to study hysteretic effects CC simulations using lattices of different sizes and various values of τ_W have been performed. Since the measurement in time (τ_M) has to be reduced in order to observe hysteretic effects, results are averaged over several $(10 - 100)$ different loops, depending on the lattice size, in order to obtain acceptable statistics.

Figure 2 shows a plot of θ_{CO} vs. $< P_{CO} >$ as obtained using $L = 32LU$, $\tau_W = 50$ MCS, and $\tau_M = 50$ MCS. For this small lattice size the relaxation time is quite short, so that hysteretic effects are absent. This result is in agreement with similar measurements performed applying the CC ensemble to the ZGB model [11]. Note that a narrow vertical region close to the center of the loop for ($< P_{CO} > \approx 0.35$) can also be observed in figure 2. On the other hand, the L-dependent upper spinodal point (P_{CO}^{US}) can also clearly be observed as shown in figure 2. On increasing the lattice size ($L = 64LU$, in figure 3), the onset of hysteretic effects can be observed for $\tau_W = 75$ MCS (figure 3(a)), while such effects become almost negligible if the waiting time is increased (figure 3(b) for $\tau_W = 400$ MCS). Furthermore, as in the case of figure 2, a vertical region located at the center of the loop and slightly above $< P_{CO} > \approx 0.35$ can be observed in figure 3(a). Also notice that such region becomes well defined when τ_W is increased (figure 3(b)).

On increasing the lattice the hysteretic effects can be observed even taking larger

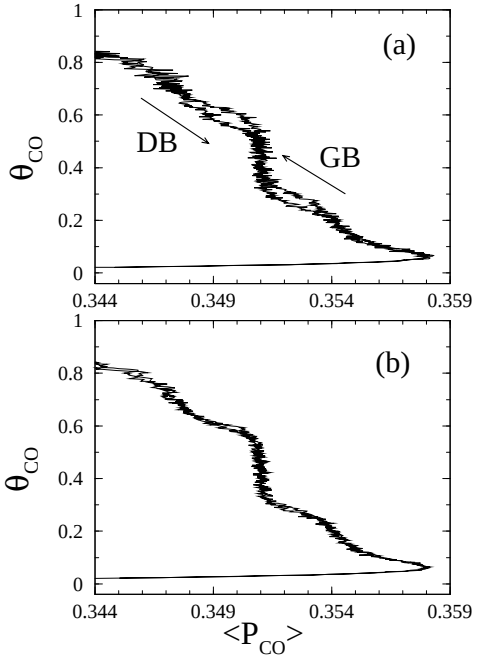


Figure 3: Plots of θ_{CO} versus $< P_{CO} >$ obtained using the CC ensemble with $L = 64$ LU, and (a) $\tau_W = 75$ MCS, $\tau_M = 50$ MCS and (b) $\tau_W = 400$ MCS, $\tau_M = 100$ MCS. The arrows pointing up and down, in figure (a), show the growing and decreasing branches (GB and DB) of the loop, respectively. More details in the text.

values of τ_W. In fact, for $L = 128LU$ (figure 4(a)) and $L = 256$ (figure 4(b)), hysteresis is still observed for $\tau_W = 1700$ MCS and $\tau_W = 2700$ MCS respectively.

It should be noticed that the loop becomes narrow when the lattice size is increased, as follows from the comparison of figures (3) and (4). Comparing these figures it also becomes evident that while the location of P_{CO}^{US} is shifted systematically toward lower values when L is increased, the location of the vertical region (close to the center of the loops) remains almost fixed very close to $P_{CO} = 0.3515$ (see figure 4(b)).

The evaluation of a CC loop for $L = 1024LU$ requires huge CPU resources, so we have restricted ourselves to the case $\tau_W = 600$ MCS and $\tau_M = 700$ MCS, since considerably larger values of τ_M became prohibitive. In this case (figure 5) hysteretic effects are quite evident and also, the growing and decreasing branches of the loops are almost vertical. However, the vertical region at the center of the loop, previously observed using smaller lattices, is no longer found.

In order to gain insight into the behavior of the system close to coexistence it is useful to analyze snapshot configurations, as shown in figure 6. Snapshots are obtained for some relevant points as indicated in figure 4(a). Just at the upper spinodal point (figure 6(a)) one observes that the active phase remains homogeneous but the nucleation of few CO-

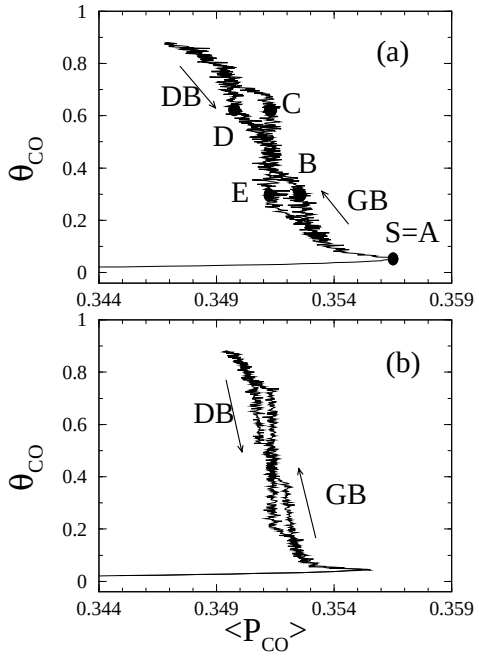


Figure 4: Plots of θ_{CO} versus $< P_{CO} >$ obtained using the CC ensemble and taking: (a) $L = 128$ LU, $\tau_W = 1700$ MCS, and $\tau_M = 300$ MCS. The points labeled A, B, C, D and E correspond to the coverages used to obtain the snapshot configurations shown in figure 6 (a)-(e), respectively. (b) $L = 256$ LU and $\tau_W = 2700$ MCS and $\tau_M = 300$ MCS.

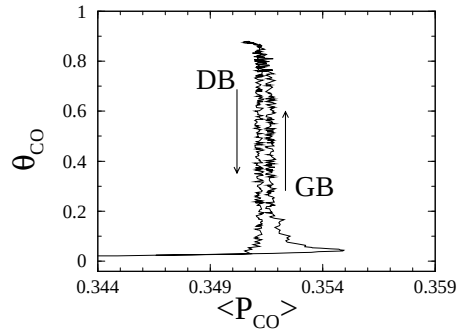


Figure 5: Plots of θ_{CO} versus $< P_{CO} >$ obtained using the CC ensemble for (a) $L = 1024$ LU, and $\tau_W = 600$ MCS, and $\tau_M = 700$ MCS.

clusters has already started. The biggest one (close to the lower right hand side in figure 6(a)) is compact (except for the presence of few N-atoms embedded into the bulk of the CO-cluster) and has reached the critical nucleation size. At the upper spinodal point one has $\theta_{CO} \approx 0.045$. On increasing the CO coverage this critical nucleus grows up into a solid and compact CO cluster surrounded by the (homogeneous) active phase, as shown in figure 6(b). The coverage with CO has increased up to $\theta_{CO} \approx 0.28$, the compact CO cluster does not percolate and its interface is essentially convex. Further increasing θ_{CO} causes the CO cluster to percolate along one direction of the sample, figure 6(c). The hysteresis loop also changes for the growing branch (as in figure 6(b)) to the central region with $\theta_{CO} \approx 0.63$ in figure 6(c). The percolating cluster is quite stable and has an interface essentially flat with a length of the order of $2L$. An additional growth of CO coverage causes the CO cluster to percolate along both directions of the lattice (figure 6(d)). Here the interface of the cluster is essentially concave and the active phase is surrounded by the massive cluster. Since the coverage with CO is the same ($\theta_{CO} \approx 0.63$) in both figures 6(c) and 6(d), the presence of hysteretic effects has to be related to the curvature of the interface of the CO cluster. Subsequently, on decreasing θ_{CO} one observes the formation of a CO cluster that percolates along only one direction of the sample (figure 6(e)). Such kind of clusters are observed along the vertical region and are characterized by an almost flat interface with an infinite effective curvature radius. Notice that despite the fact that the CO coverage is the same in both figures 6(b) and 6(e) ($\theta_{CO} \approx 0.28$), the curvature of the interface of the CO cluster is quite different and hysteretic effects are observed (see figure 4(a)).

Summing up, the sequence of snapshots shown in figure 6, as well as additional figures not shown here for the sake of space, allows us to infer the following behavior of the interface of the CO cluster along the hysteresis loop: between the spinodal point and the growing branch the curvature radius of the interface is positive and finite. Along the vertical region the radius of curvature is infinite, while within the decreasing branch the radius of curvature is negative and finite. Almost horizontal regions observed in the loops correspond to regions where the curvature radius crosses over between two different behaviors.

In order to quantitatively analyze the behavior of P_{CO} corresponding to the different branches and the vertical region, it is assumed that the growing (decreasing) branch starts at the point where both curves merge (split out). Figure 7 shows the dependence of the location of the growing branch and the decreasing branch (P_{CO}^{GB} and P_{CO}^{DB}, respectively) on the inverse of the lattice size. The $L-$dependence of P_{CO} at the vertical region (P_{CO}^{VR}) has also been included for the sake of comparison.

As already discussed the location of all relevant points, namely P_{CO}^{X} with $X = GB, DB$ and VR depend on the curvature radius (s) of interface of the massive CO cluster. Such dependence can be written as follows:

$$P_{CO}^{X} = P_{CO}^{X}(L \to \infty) + F^{X}(s), \tag{6}$$

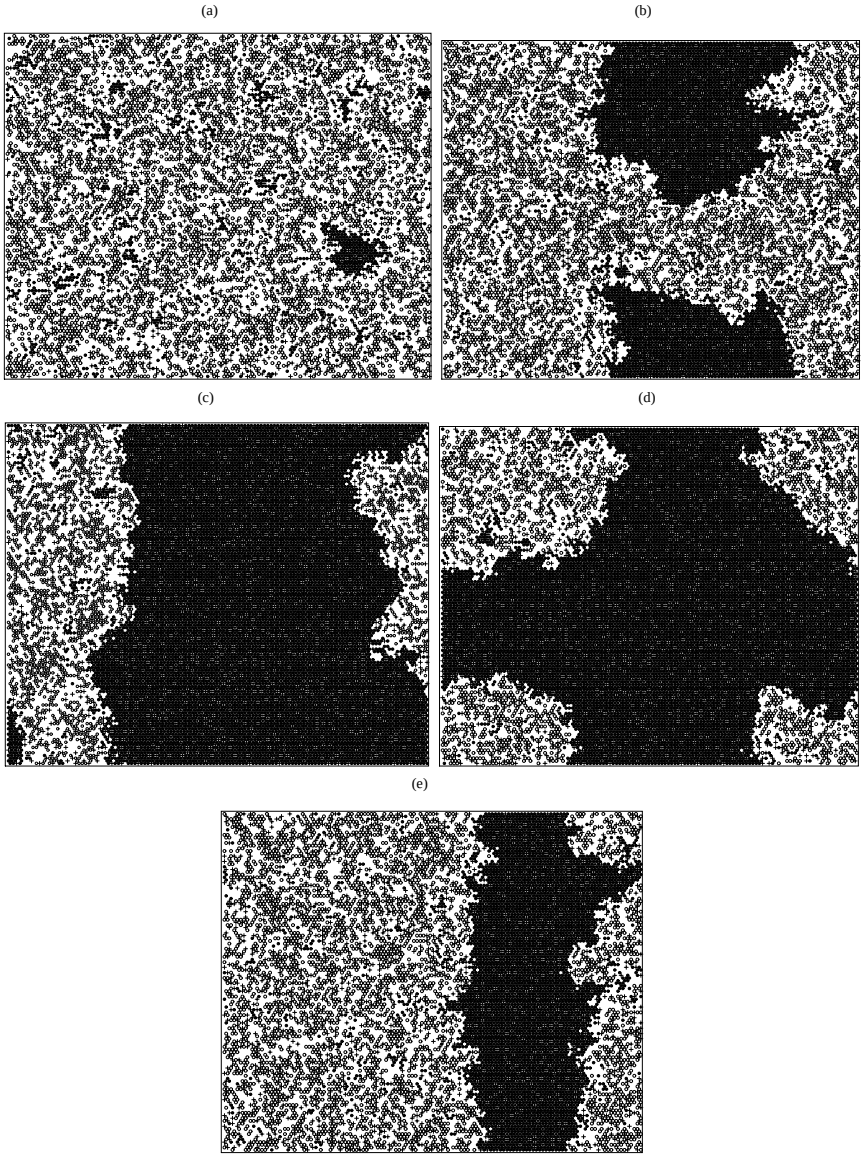


Figure 6: Typical snapshot configurations obtained using the CC ensemble close to coexistence for $L = 128$ LU and the points A, B, C, D and E shown in figure 4(a). (a) Snapshot corresponding to the upper spinodal point S≡A, (b) and (d) snapshots corresponding to the points B and D respectively. (c) and (e) CO-percolating clusters obtained in the central region (points C and E respectively). Here ∘ denotes O(ad), +denotes N(ad) and • denotes CO(ad).

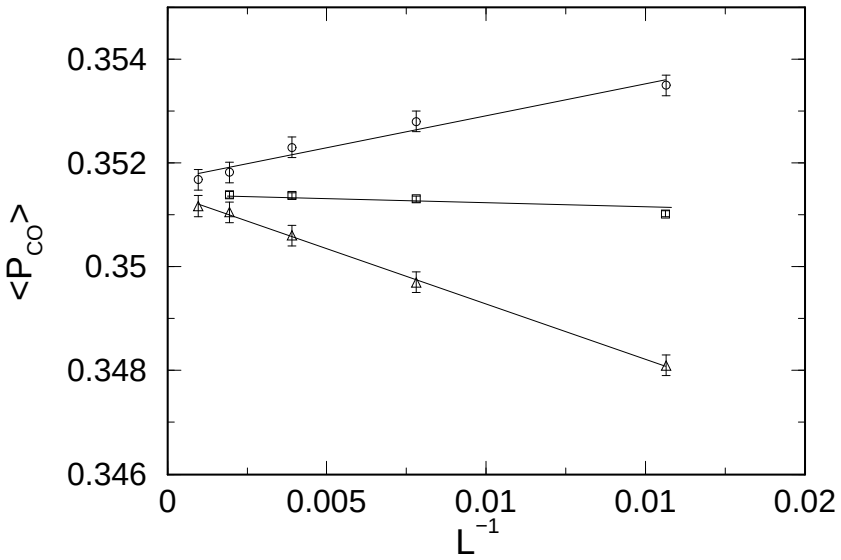


Figure 7: Plots of $< P_{CO} >$ versus L^{-1} measured in the growing branch (◯), decreasing branch (△), and the vertical region (□). The straight lines correspond to the best fits of the data that extrapolate to $L \to \infty$. L is measured in LU.

where $P_{CO}^{X}(L \to \infty)$ is the location of the point under consideration after proper extrapolation to the thermodynamic limit and $F(s)$ is an s-dependent function. For the vertical region one has $s \to \infty$ and P_{CO}^{VR} is almost independent of L, so $F^{VR}(\infty) \to 0$, as shown in figure 7. In contrast, for the DB and the GB , s is finite and of the order of $-1/L$ and $1/L$, respectively. So, one has $F^{DB}(s) \approx -A/L$ while $F^{GB}(s) \approx B/L$. All these arguments can be confirmed by the results shown in figure 7 and the extrapolated points are:

$$P_{CO}^{GB}(L \to \infty) = 0.3514(3),$$
$$P_{CO}^{DB}(L \to \infty) = 0.3517(3),$$
$$P_{CO}^{VR}(L \to \infty) = 0.35145(5),$$

respectively. Also, $A \approx 0.215(5)$ and $B, \approx 0.12(2)$ are obtained.

The observed behavior allows us to identify $P_{CO}^{VR}(L \to \infty)$ as the coexistence point $P_{CO}^{Coex} \cong 0.35145(5)$ in excellent agreement with the value $P_{CO} = 0.35140(1)$ reported by Brosilow and Ziff ([12]).

This result is in contrast with measurements performed with the ZGB model. In fact, for the ZGB systems the vertical region is not observed while the locations of the growing and decreasing branches are almost independent of the lattice size [11]. Consequently, the CC ensemble does not provide a method suitable for the location of the coexistence point that has to be estimated using the spontaneous creation method [11]. It is expected that

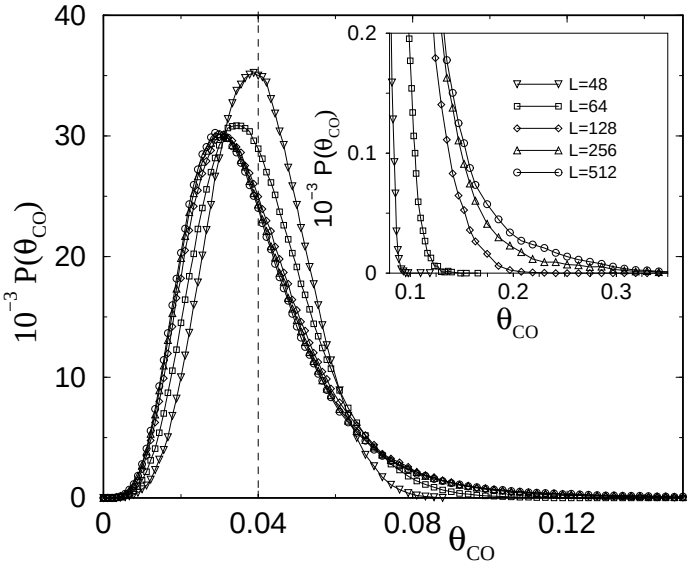


Figure 8: Plots of the *local CO*−coverage fluctuations ($P(\theta_{CO})$) versus θ_{CO} measured using the constant coverage ensemble keeping the *global CO* coverage at $\theta_{CO} = 0.040$ and using lattices of different sizes as indicated in the figure, where L is measured in LU. The inset shows a detailed view of the right-hand side of the distributions. Results averaged over 3×10^6 different configurations.

the difference observed between the models may be due to the different behavior of the interface of the massive CO cluster. So, we are planning to perform extensive simulations on this subject to clarify this open question.

Pointing our attention to the upper spinodal point, it is found that its location depends on the lattice size, so $P_{CO}^{US}(L)$ can be determined from the loop, as shown in figures (2-4). It is expected that this dependence of $P_{CO}^{US}(L)$ is due to local fluctuations of the CO coverage that take place during the nucleation of the critical cluster. In order to check this conjecture, the probability distribution of the *local CO* coverage ($P(\theta_{CO})$) in small patches of side $L_o = 30LU$ was measured for lattices of different sizes. It should be noticed that, in order to perform these measurements, the CC algorithm that keeps the *global* coverage of CO almost constant has been used. Setting $\theta_{CO} = 0.040$, i.e. a value slightly smaller than the coverage at the upper spinodal point, the probability distributions shown in figure 8 have been obtained. For a rather small lattice ($L = 48$ in figure 8) $P(\theta_{CO})$ is almost symmetric around the maximum $\theta_{CO}^{max} \approx \theta_{CO} = 0.040$. However, on increasing the lattice size the peak is shifted toward lower θ_{CO} values and the distribution function is clearly asymmetric. While the left-hand side remains practically independent of finite size effects (say for $L \geq 128$ LU), an increasingly long tail emerges on the right hand side of the distribution (for a detailed view see the inset of figure 8). The existence of these non-vanishing tails implies that fluctuations of the *local CO* coverage up to relatively

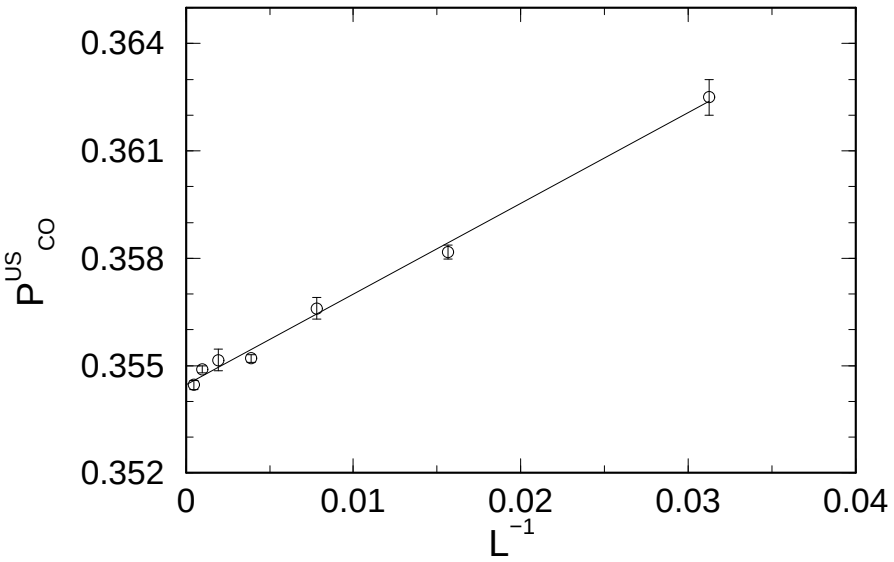


Figure 9: Plots of P_{CO}^{US} versus L^{-1}, where L is measured in LU. The straight line corresponds to the best fit of the data that extrapolates to $P_{CO}^{US}(L \to \infty) = 0.3544(2)$.

large values are present in larger samples. Such excursions of the coverage induce the nucleation of critical CO clusters in larger lattices for smaller adsorption probabilities of CO, consequently $P_{CO}^{US}(L)$ must decrease upon increasing L. In fact, figure 9, which shows a plot of $P_{CO}^{US}(L)$ versus L^{-1}, confirms this trend. As a first approximation the data can be fitted by a straight line that gives $P_{CO}^{US}(L \to \infty) \cong 0.3544(2)$. Furthermore our estimate for the coverage is $\theta_{CO}^{US} \cong 0.043(1)$. These results point out that in the thermodynamic limit the spinodal point is very close to coexistence, i.e. $\Delta\, P_{CO} = P_{CO}^{US} - P_{CO}^{Coex} \cong 0.003$. For the sake of comparison it is worth mentioning that for the ZGB model one has $\Delta\, P_{CO} \cong 0.0012$ [11].

3.2 Epidemic Study.

In order to perform epidemic studies it is necessary to account for the fact that the poisoned (absorbing) state above coexistence is non-unique, since it is due to a mixture of CO and N atoms with coverage $\theta_{CO} \approx 0.9$ and $\theta_N \approx 0.1$, as shown in figure 1. So, the starting configuration has to be obtained running the actual dynamics of the system slightly above coexistence until 'natural' absorbing states suitable for the studies are generated.

Extensive epidemic simulations ($\sim 2\text{x}10^9$ different runs) have been performed for the following values of P_{CO}: P_{CO}^{Coex}, P_{CO}^{US}, $P_{CO}^{DB}(L = 256LU)$ and $P_{CO}^{GB}(L = 256LU)$. A value close to coexistence but slightly inside the active region, namely $P_{CO} = 0.347$, has also been used. The obtained results can be observed in figure 10, which shows log-log plots

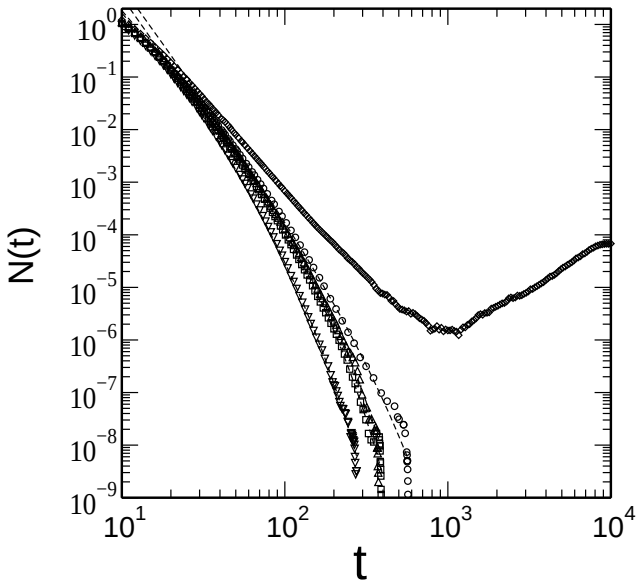


Figure 10: Log-log plots of the number of vacant sites $N(t)$ versus t; measured in MCS; for epidemic simulations performed using lattices of size $L = 256$ LU. Results averaged up to 3x10^9 different runs (triangle down) $P_{CO}^{US} = 0.3544$, ($\square$) $P_{CO}^{GB} = 0.3522$, ($\triangle$)$P_{CO}^{Coex} = 0.35145$, ($\bigcirc$) $P_{CO}^{DB} = 0.3506$ and ($\Diamond$) $P_{CO} = 0.3470$) .

of $N(t)$ versus t. It becomes evident that the method is quite sensitive to tiny changes of P_{CO}. The obtained curves are fitted by equation (5), as shown in figure 10 for P_{CO}^{Coex}. The best fits are obtained for the parameters listed in Table I.

It is concluded that close to coexistence one has $\eta_{eff} \cong 3.5 \pm 0.5$ with a characteristic time $T \sim 50$ MCS except for $P_{CO} = 0.3506$ with $T \sim 160$ MCS, a result that may reflect the fact that this point actually lies within the active region of the phase diagram. In fact, in the active region larger T values are expected, as judged by the results shown in figure 10.

Of course, one may obtain better fits using different scaling ansatz than that in equation (5). Our main finding, however, is that the occurrence of a power-law scaling behavior close to coexistence can unambiguously be ruled out. This result is in qualitative agreement with recent numerical data obtained with the ZGB model [11]. All these observations are also in agreement with the experience gained studying first-order reversible phase transitions where it is well established that correlations are short ranged, preventing the emergency of scale invariance.

Let us now point our attention to the run performed taking $P_{CO} = 0.347$ (figure 10). A rapid decrease in $N(t)$ up to 10^3 MCS due to the low survivability of the initial empty patch is observed. However, for $t > 10^3$ MCS only few epidemics survive (actually around 10 epidemics over 10^9) and the average number of empty sites increases according to $N(t) \propto t^2$, indicating the homogeneous propagation of the epidemic. For $t \sim 10^4$ MCS

the active region covers the whole sample and the average density of empty sites remains stationary close to $\theta_{emp} \approx 0.52$.

P_{CO}	η_{eff}	T MCS	Number of epidemics
$P_{CO}^{GB} = 0.3506$	4.2 ± 0.2	159 ± 10	4.3x10^9
$P_{CO}^{Coex} = 0.35145$	3.45 ± 0.05	58 ± 1	2.5x10^9
$P_{CO}^{DB} = 0.3522$	3.38 ± 0.01	50 ± 1	3.5x10^9
$P_{CO}^{US} = 0.3544$	4.1 ± 0.1	40 ± 4	5.5x10^9

Table I Caption. Results obtained fitting the data corresponding to different values of P_{CO}, shown in figure 10, using equation (5).

4 Conclusions and outlook.

In summary, after an extensive Monte Carlo simulation study of the first-order irreversible phase transition of the YK model for the catalized NO+CO reaction we concluded that: i) hysteretic effects are found around the coexistence using the constant-coverage ensemble. The hysteresis loop basically exhibits three characteristic regions: a growing branch (GB), a vertical region (VR) and a decreasing branch (DB). Within each region the massive CO cluster corresponding to the inactive phase has a well defined convex (GB), concave (DB) and flat (VR) curvature. We are planning to study the dynamics of such interface in order to clarify the interplay between hysteresis and interfacial properties such as effective surface tension, roughness, curvature, etc. ii) The VR of the loop can be identified as the coexistence point. iii) The CC loop also gives evidence of a lattice size dependent upper spinodal point that can be extrapolated to the thermodynamic limit. Recently [20] one of us has shown that the spinodal point can be located quite accurately performing studies of the short-time dynamics of the system. So, we are planning to perform similar studies using the YK model in order to obtain an independent measurement of the upper spinodal point. iv) Epidemic studies reveal the existence of short ranged correlations close to coexistence.

Based on these findings and the experience gained studying a similar system (namely the ZGB model [11]), we concluded that first-order irreversible phase transitions share many characteristics with their equilibrium (reversible) counterpart. So, we expect that these results will contribute to the development of a theoretical frame for the description of irreversible critical behavior.

ACKNOWLEGMENTS: This work was supported by CONICET, UNLP, and AN-

PCyT (ARGENTINA). E. L. acknowledges the CIC for the provision of a study fellowship.

References

[1] Patrykiejew A., Sokolowski S. and Binder K., Surface Science Reports **37**, 207-344 (2000).

[2] Marro J. and Dickman R. *Nonequilibrium Phase Transitions in Lattice Models* Cambridge University Press, Cambridge (U.K.), 1999.

[3] Imbihl R., Prog. Surf. Sci. **44**, 185 (1993); Ertl G., Adv. Catal. **37**, 213 (1990).

[4] Yaldram, K. and Khan M. A., J. Catal. **131**, 369 (1991).

[5] Albano E. V., Heter. Chem. Rev. **3**, 389 (1996).

[6] Albano E. V., *Surface Chemical Reactions*, in "Computational methods in Surface and Colloid Science", M. Borówko (Ed.), Marcel Dekker, Inc. New York, 2000. Page 387.

[7] Ziff R., Gulari E., and Barshad Y. Phys. Rev. Lett. **56**, 2553 (1986).

[8] Christmann K., *Introduction to Surface Physical Chemistry* Steinkopff Verlag, Darmstadt, 1991, pp. 1-274.

[9] Ehsasi M. et al., J. Chem. Phys. **91**, 4949 (1989).

[10] Berdau M. et al., J. Chem. Phys. **110**, 11551 (1999).

[11] Monetti R. A. and Albano E. V., J. Phys. A: Math. Gen.**34**, 1103 (2001).

[12] Brosilow B. J. and Ziff R. M., J. Catal. **136**, 275 (1992).

[13] Meng B., Weinberg W. H. and J. W. Evans, Phys. Rev. E. **48**, 3577 (1993).

[14] Meng B., Weinberg W. H. and J. W. Evans, J. Chem. Phys. **101**, 3234 (1994).

[15] Dickman A. G., Grandi B. C., Figueiredo W. and Dickman R., Phys. Rev. E.**59**, 6361 (1999).

[16] Ziff R. and Brosilow B. J., Phys. Rev. A.; **46**, 4630 (1992).

[17] T. Tomé and M. J. de Oliveira. Phys. Rev. Lett., **86**, 5643 (2001).

[18] Grassberger P. and de la Torre A., Ann. Phys. (New York) **122**, 373 (1979); Grassberger P., J. Phys A: *Math Gen* **22**, 3673 (1989).

[19] Jensen I., Fogedby H., and Dickman R., Phys. Rev. A **41**, R3411 (1990). Voigt C. A. and Ziff R. M., Phys. Rev. E **56**, R6241 (1997).

[20] Albano E. V., Phys. Lett. A. **288**, 73 (2001).